Geometrical percolation threshold of congruent cuboidlike particles in overlapping particle systems

Jianjun Lin,[1] Huisu Chen,[1,*] and Wenxiang Xu[2,†]

[1]*Jiangsu Key Laboratory of Construction Materials, School of Materials Science and Engineering, Southeast University, Nanjing 211189, People's Republic of China*

[2]*Institute of Materials and Structures Mechanics, College of Mechanics and Materials, Hohai University, Nanjing 211100, People's Republic of China*

(Received 4 May 2018; published 25 July 2018)

With the advances in artificial particle synthesis, it is possible to create particles with unique shapes. Particle shape becomes a feasible parameter for tuning the percolation behavior. How to accurately predict the percolation threshold by particle characteristics for arbitrary particles has aroused great interest. Towards this end, a versatile family of cuboidlike particles and a numerical contact detection algorithm for these particles are presented here. Then, combining with percolation theory, the continuum percolation of randomly distributed overlapping cuboidlike particles is studied. The global percolation threshold ϕ_c of overlapping particles with broad ranges of the shape parameter m in [1.0, $+\infty$) and aspect ratio a/b in [0.1, 10.0] is computed via a finite-size scaling technique. Using the generalized excluded-volume approximation, an analytical formula is proposed to quantify the dependence of ϕ_c on the parameters m and a/b, and its reliability is verified. The results reveal that the percolation threshold ϕ_c of overlapping cuboidlike particles is heavily dependent on the shapes of particles, and much more sensitive to a/b than m. As the cuboidlike particles become spherical (i.e., $m = 1.0$ and $a/b = 1.0$), the maximum threshold $\phi_{c,\max}$ can be obtained.

DOI: 10.1103/PhysRevE.98.012134

I. INTRODUCTION

Percolation behavior of particle systems is one of the most popular research topics in statistical physics [1,2] and closely related to a host of physical and chemical phenomena in materials science such as electrical properties of conductive composites [3,4], cluster formation in ethanol-water mixtures [5], recharge of groundwater in aquifers [6], metal-insulator transition in condensed matter systems [7], penetration of deleterious ions in porous structures [8], and ductile-brittle transition of amorphous alloys [9]. Percolation threshold is a mathematical concept related to the formation of long-range connectivity in multiphase materials [10], and can be characterized by the critical covering fraction of particles in particle systems. With the emergence of global connectivity in the systems, the materials performance would be changed dramatically. Therefore, the investigations on continuum percolation of particle structures, especially the percolation threshold, have attracted appreciable attention in recent years [11]. Accurate prediction of percolation threshold has been a central task in the study of percolation behavior and the associated properties of a great deal of composite materials.

Over the past decades, there has been significant progress in the synthesis of particles with unique shapes such as ellipsoids [12–17], polyhedrons [18–20], stars [21], cubelike particles [22–24], nonconvex particles [25], etc. The advances in artificial particle synthesis lead to new possibilities for applications where particle shape is a crucial influencing factor, like the aforementioned percolation behavior of particle systems. However, previous works on the percolation phenomena of particles mainly focused on the random packing of spheres [26–28], fibers [29], disks [30], ellipsoids [31–33], spherocylinders [34,35], and hyperparticles [36]. In this study, a versatile family of cuboidlike particles [37–39] which smoothly interpolate between ellipsoids and cuboids is introduced. These particles are able to capture many of the essential features of real particle shapes and represent a wide range of shapes in nature. This has aroused great interest of investigating the microstructure and performance of the cuboidlike particle systems. As described by Eq. (1), the surface of cuboidlike particles, also known as "superellipsoids," can be simply described by an extension of the equation for an ellipsoid.

$$\frac{|x|^{2m}}{a^{2m}} + \frac{|y|^{2m}}{b^{2m}} + \frac{|z|^{2m}}{c^{2m}} = 1, \tag{1}$$

where a, b, and c are three semimajor axis lengths in the direction of the x, y, and z axes, respectively; m is a shape parameter that can vary between 1.0 and $+\infty$ corresponding to ellipsoids ($m = 1.0$) and cuboids ($m = +\infty$). Figure 1 illustrates the morphologies of the cuboidlike particles with different values of the parameter m and the aspect ratio a/b, where the semimajor axis length c is equal to the length b (i.e., $b = c$).

As mentioned above, a considerable amount of research on the quantitative relations between particle shapes and the percolation threshold for nonspherical particles can be found in the literature [29–36]. Because there have been few systematical reports on these cuboidlike particles, we chose to study the dependence of percolation threshold of overlapping

*chenhs@seu.edu.cn
†xwxfat@gmail.com

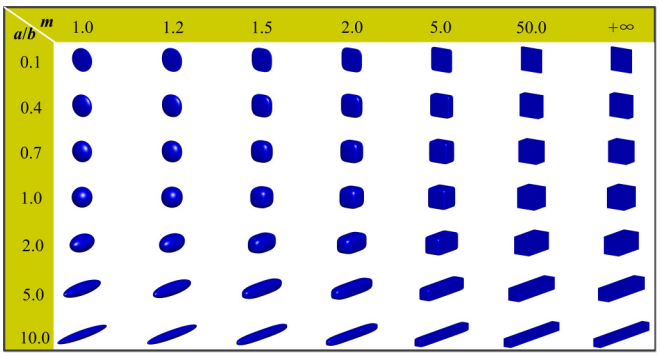

FIG. 1. The morphologies of cuboidlike particles with different m and a/b.

particle systems on the geometric characteristics of cuboidlike particles, such as the shape parameter m and the aspect ratio a/b.

To achieve the above goal, both the geometrical model and the contact detection algorithm for the cuboidlike particles are given first. By using the Monte Carlo method, the percolation models of overlapping cuboidlike particles are generated, and a searching algorithm of percolation in finite-size structures is presented in detail. The percolation transition width ΔL, correlation-length critical exponent ν, and percolation threshold ϕ_c are determined successively via an extensive finite-size scaling analysis technique. Based on the simulated results, the generalized excluded-volume approximation is utilized here to derive an analytical formula for the global percolation threshold ϕ_c of cuboidlike particles, which can be used to predict the value of ϕ_c for wide ranges of m in [1.0, $+\infty$) and a/b in [0.1, 10.0]. The reliability of the analytical solutions from the present study is further verified by comparing with the data in the literature.

II. CONTINUUM PERCOLATION

Percolation mainly describes the behavior of connected clusters in random systems. In the modeling of continuum percolation in particulate media, the structures are generally assumed to be composed of random packing of soft particles [26,31,32,35]. In the system, if two particles contact, they are defined as overlapping particles and identified to the same cluster. If there is one cluster which could continuously span the domain from one boundary to its opposite boundary, the percolation is deemed to be realized in the whole system. Before investigating the percolation of cuboidlike particles, two issues still need to be dealt with: The first one is how to describe the geometrical model of the cuboidlike particle with arbitrary position, size, and orientation by a general function, and the second one is how to efficiently detect the interparticle contact in the packing systems of cuboidlike particles.

A. Geometrical model of cuboidlike particle

Formally speaking, the function, i.e., Eq. (1), can only describe the cuboidlike particle with its center located at the origin of the Cartesian coordinates and three semimajor axes parallel to the coordinate axes. To characterize these nonspherical particles with random positions, sizes, and orientations, a so-called ten-parameter method is used by referring to the model of ellipsoids [40]. In this approach, a random cuboidlike particle in three-dimensional (3D) space can be represented by ten degrees of freedom, i.e., center (x_0, y_0, z_0), three semimajor axis lengths (a, b, c), three Euler angles (α, β, γ), and shape parameter (m). The corresponding geometrical function of cuboidlike particles can be expressed as below:

$$X_{\text{int}} \begin{bmatrix} 1 & 0 & 0 & 0 \\ 0 & 1 & 0 & 0 \\ 0 & 0 & 1 & 0 \\ 0 & 0 & 0 & -1 \end{bmatrix} X_{\text{int}}^T = 0, \tag{2}$$

where $X_{\text{int}} = (x_{\text{int}}^m, y_{\text{int}}^m, z_{\text{int}}^m, 1)$. x_{int}, y_{int}, and z_{int} are three intermediate variables, and can be obtained by Eq. (3).

$$(xyz1)^T = TRS(x_{\text{int}} y_{\text{int}} z_{\text{int}} 1), \tag{3}$$

where (x, y, z) are the coordinates of an arbitrary point on the surface of cuboidlike particles; T, R, and S are the translation, rotation, and scaling matrices, which can be expressed by Eqs. (4)–(6), respectively.

$$T = \begin{bmatrix} 1 & 0 & 0 & x_0 \\ 0 & 1 & 0 & y_0 \\ 0 & 0 & 1 & z_0 \\ 0 & 0 & 0 & 1 \end{bmatrix}, \tag{4}$$

$$R = \begin{bmatrix} \cos\gamma & -\sin\gamma & 0 & 0 \\ \sin\gamma & \cos\gamma & 0 & 0 \\ 0 & 0 & 1 & 0 \\ 0 & 0 & 0 & 1 \end{bmatrix} \begin{bmatrix} \cos\beta & 0 & \sin\beta & 0 \\ 0 & 1 & 0 & 0 \\ -\sin\beta & 0 & \cos\beta & 0 \\ 0 & 0 & 0 & 1 \end{bmatrix} \begin{bmatrix} 1 & 0 & 0 & 0 \\ 0 & \cos\alpha & -\sin\alpha & 0 \\ 0 & \sin\alpha & \cos\alpha & 0 \\ 0 & 0 & 0 & 1 \end{bmatrix}, \tag{5}$$

$$S = \begin{bmatrix} a & 0 & 0 & 0 \\ 0 & b & 0 & 0 \\ 0 & 0 & c & 0 \\ 0 & 0 & 0 & 1 \end{bmatrix}. \tag{6}$$

B. Contact detection of cuboidlike particles

In general, the numerical contact detection algorithms for nonspherical particles can be categorized into two kinds: the multisphere technique [41,42] and the analytical geometric approach [15,18,21]. Compared with the first method, the analytical geometric approach generally has more accuracy and efficiency. In this approach, the surface of the nonspherical particle is characterized by the analytical model and the interparticle contact is detected by means of the mathematical principle. In this section, we present a simple interparticle contact detection algorithm based on the characteristics of these cuboidlike particles with arbitrary shapes.

Two random cuboidlike particles i and j with the same parameter m are expressed by Eqs. (2)–(6) with ten degrees of freedom as $(x_{0,i}, y_{0,i}, z_{0,i}, a_i, a_i, b_i, c_i, \beta_i, \gamma_i, m)$ and $(x_{0,j}, y_{0,j}, z_{0,j}, a_j, b_j, c_j, \alpha_j, \beta_j, \gamma_j, m)$, respectively. The translation, rotation, and scaling matrices of particles i and j are denoted by T_i, R_i, and S_i, and T_j, R_j, and S_j, respectively. Assume that the maximum and minimum distances between the center of a random particle and its corresponding surface

are denoted by $d_{\max}$ and $d_{\min}$. Then, the contact between particle i and particle j can be preliminarily detected by Eqs. (7) and (8).

If the central distance d_{ij} between these two cuboidlike particles meets Eq. (7), no contact occurs.

$$d_{ij} = \sqrt{(x_{0,i} - x_{0,j})^2 + (y_{0,i} - y_{0,j})^2 + (z_{0,i} - z_{0,j})^2} > d_{\max,i} + d_{\max,j}. \tag{7}$$

If the central distance d_{ij} satisfies Eq. (8), contact must exist.

$$d_{ij} = \sqrt{(x_{0,i} - x_{0,j})^2 + (y_{0,i} - y_{0,j})^2 + (z_{0,i} - z_{0,j})^2} \leqslant d_{\min,i} + d_{\min,j}. \tag{8}$$

It is worth noting that, for the cuboidlike particles with m in $[1.0, +\infty)$, the minimum distance $d_{\min}$ can be easily obtained by Eq. (9).

$$d_{\min} = \min(a, b, c). \tag{9}$$

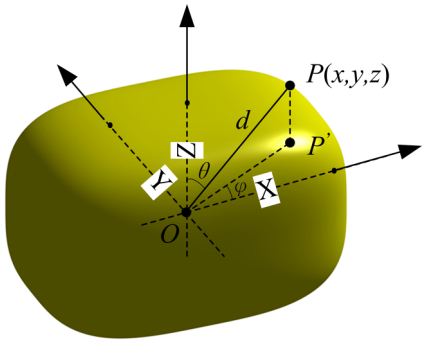

FIG. 2. A random point $P(x,\ y,\ z)$ on the surface of cuboidlike particle.

However, the maximum distance $d_{\max}$ is determined by both the shape parameter (m) and three semimajor axis lengths $(a,\ b,\ c)$, and can not be described by an analytical function. Thus, a searching algorithm of infinite approximation is proposed here to derive the value of $d_{\max}$ for an arbitrary cuboidlike particle. As shown in Fig. 2, taking one cuboidlike particle expressed by Eq. (1) as an example, a random point $P(x,\ y,\ z)$ on the surface of this particle can be described by Eq. (10).

$$x = d(\theta, \varphi)\sin\theta\cos\varphi, \tag{10a}$$

$$y = d(\theta, \varphi)\sin\theta\sin\varphi, \tag{10b}$$

$$z = d(\theta, \varphi)\cos\theta, \tag{10c}$$

$$d(\theta, \varphi) = \frac{abc}{(b^{2m}c^{2m}|\sin\theta|^{2m}|\cos\varphi|^{2m} + a^{2m}c^{2m}|\sin\theta|^{2m}|\sin\varphi|^{2m} + a^{2m}b^{2m}|\cos\theta|^{2m})^{1/(2m)}}, \tag{10d}$$

where θ is the angle between the zenith direction and the line segment OP, φ is the signed angle measured from the azimuth reference direction to the orthogonal projection OP' of the line segment OP on the reference plane O-XY, and $d(\theta, \varphi)$ represents the distance from the surface point P to the origin O.

It can be seen from Eq. (10d) that for a cuboidlike particle with preselected shape parameter (m) and semimajor axis lengths (a, b, c), the value of $d(\theta, \varphi)$ is closely related to the angles θ and φ. Due to symmetry of the particle in Fig. 2, we only need consider the surface of the cuboidlike particle in the first quadrant to derive the maximum distance $d_{\max}$. As shown in Fig. 3, the values of both θ and φ are in the interval of $[0,\ \pi/2]$. Suppose the angle φ is equal to a fixed value φ_k in the interval of $[\varphi_{\min},\ \varphi_{\max}]$ first. The corresponding points with φ_k and θ on the surface of the particle will form a red curve (seen in Fig. 3), and the maximum distance from the origin O to the red curve is denoted by the symbol $d_{\max}^{\varphi_k}$. Consequently, $d_{\max}$ is equivalent to the largest value of a series of distances $d_{\max}^{\varphi_k}$ from the origin O to all of these surficial curves in 3D space, which can be mathematically described by Eq. (11).

$$d_{\max} = \max\left\{d_{\max}^{\varphi_k}\right\} \quad \varphi_k \in [\varphi_{\min}, \varphi_{\max}]. \tag{11}$$

Next, the major challenge we faced was how to obtain the value of $d_{\max}^{\varphi_k}$ for an arbitrary curve with φ_k on the surface of the particle as well as the corresponding angle θ. According to the golden section searching algorithm [43], an approximation method involved with θ and φ is proposed. As shown in Fig. 3, the initial minimum value $(\theta_{\min})$ and a maximum value $(\theta_{\max})$ are set to 0 and $\pi/2$, respectively. Obviously, the angle θ corresponding to the distance $d_{\max}^{\varphi_k}$ must exist between $\theta_{\min}$

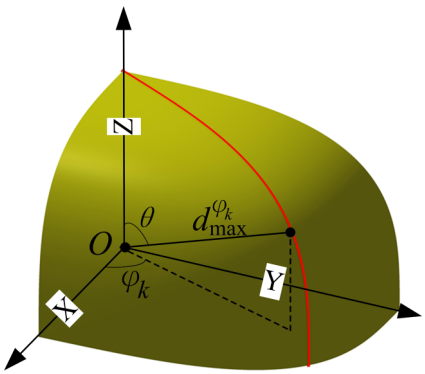

FIG. 3. Schematic diagram of an arbitrary curve with a fixed angle φ_k on the surface of cuboidlike particle in the first quadrant.

and $\theta_{\max}$. Then, two prescribed angles θ_1 and θ_2 in the interval of $[\theta_{\min},\ \theta_{\max}]$ are obtained by Eqs. (12) and (13).

$$\theta_1 = \theta_{\min} + \kappa(\theta_{\max} - \theta_{\min}), \tag{12}$$

$$\theta_2 = \theta_{\max} - \kappa(\theta_{\max} - \theta_{\min}), \tag{13}$$

where κ is a random value between 0 and 0.5.

The distances $d(\theta_1, \varphi_k)$ and $d(\theta_2, \varphi_k)$ are separately calculated by substituting the values of θ_1 and θ_2 into Eq. (10). According to the quantitative relation between $d(\theta_1, \varphi_k)$ and $d(\theta_2, \varphi_k)$, we can use the following rules:

If the distance $d(\theta_1, \varphi_k)$ is smaller than (or equal to) the value of $d(\theta_2, \varphi_k)$, the minimum value $(\theta_{\min})$ and maximum value $(\theta_{\max})$ are reset by Eq. (14)

$$\theta_{\min} = \theta_1, \quad \theta_{\max} = \theta_{\max}. \tag{14}$$

If the distance $d(\theta_1, \varphi_k)$ is larger than the value of $d(\theta_2, \varphi_k)$, the minimum value $(\theta_{\min})$ and maximum value $(\theta_{\max})$ are reset by Eq. (15).

$$\theta_{\min} = \theta_{\min}, \quad \theta_{\max} = \theta_2. \tag{15}$$

A reset interval of $[\theta_{\min},\ \theta_{\max}]$ can be obtained. Using Eqs. (12) and (13) again, the new interval of $[\theta_{\min},\ \theta_{\max}]$ is redivided into three parts (i.e., $[\theta_{\min},\ \theta_1)$, $[\theta_1,\ \theta_2)$, and $[\theta_2, \theta_{\max}]$). The new distances $d(\theta_1, \varphi_k)$ and $d(\theta_2, \varphi_k)$ are calculated by Eq. (10d) and compared. The above process is iterated until the angle difference between $\theta_{\max}$ and $\theta_{\min}$ meets Eq. (16).

$$|\theta_{\max} - \theta_{\min}| \leqslant \varepsilon, \tag{16}$$

where ε is a specified threshold and selected to be 1.0×10^{-5} in the study.

According to Eq. (17), the maximum distance $d_{\max}^{\varphi_k}$ from the origin O to an arbitrary curve with φ_k on the surface of cuboidlike particle (e.g., the red curve in Fig. 3) as well as the corresponding angle θ can be obtained.

$$d_{\max}^{\varphi_k} = \max\{d(\theta_1, \varphi_k), d(\theta_2, \varphi_k)\}. \tag{17}$$

The maximum distance $d_{\max}$ as shown in Eq. (11) can also be derived by the above-mentioned method on the basis of all of the acquired distances $d_{\max}^{\varphi_k}$, but the research object of the angle interval is $[\varphi_{\min}, \varphi_{\max}]$ rather than $[\theta_{\min}, \theta_{\max}]$. For the surface of the particle in Fig. 3, the initial minimum value $(\varphi_{\min})$ and the maximum value $(\varphi_{\max})$ are also set to 0 and $\pi/2$ within the first quadrant, respectively. By Eqs. (18) and (19), two prescribed angles φ_1 and φ_2 in the interval of $[\varphi_{\min}, \varphi_{\max}]$ are obtained as below:

$$\varphi_1 = \varphi_{\min} + \kappa(\varphi_{\max} - \varphi_{\min}), \tag{18}$$

$$\varphi_2 = \varphi_{\max} - \kappa(\varphi_{\max} - \varphi_{\min}). \tag{19}$$

By substituting φ_1 and φ_2 into Eq. (10d), the distances $d_{\max}^{\varphi_1}$ and $d_{\max}^{\varphi_2}$ can be separately obtained and compared. By utilizing the analogous approach expressed as Eqs. (14) and (15), a new interval of $[\varphi_{\min}, \varphi_{\max}]$ is obtained, and then redivided. The derivation process mentioned above is also iterated until the difference between $\varphi_{\max}$ and $\varphi_{\min}$ is smaller than the threshold ε as Eq. (20). Once the iteration is completed, the corresponding $d_{\max}$ can be derived by Eq. (11).

$$|\varphi_{\max} - \varphi_{\min}| \leqslant \varepsilon. \tag{20}$$

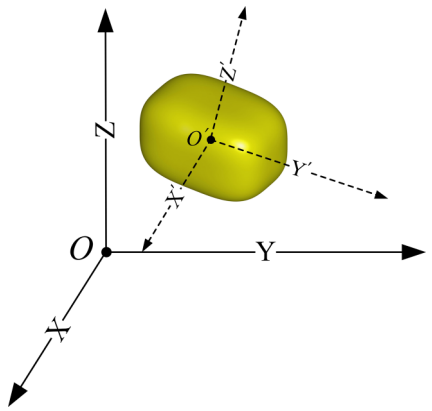

FIG. 4. Schematic diagram of the linear transformation from the global coordinate system O-XYZ to the local coordinate system O'-X′Y′Z′.

It should be noted methodologically that the total process of deriving $d_{\max}^{\varphi_k}$ for a fixed curve with φ_k is nested in the process of deriving $d_{\max}$ by narrowing down the interval of $[\varphi_{\min}, \varphi_{\max}]$ in the computer simulation. Based on the above approximation algorithm, Eq. (7) can be adopted easily by us.

In addition, if the distance d_{ij} satisfies Eq. (21), further effort is needed to detect whether or not these particles contact.

$$d_{\min,i} + d_{\min,j} < d_{ij} \leqslant d_{\max,i} + d_{\max,j}. \tag{21}$$

In previous work [44], a numerical algorithm of efficiently detecting the contact of superballs has been developed based on linear coordinate transformation. In this paper, the algorithm is extended to these cuboidlike particles. Taking the cuboidlike particle i for example, T_i and R_i are the translation and rotation matrices, respectively. According to Eq. (22), the cuboidlike particle i in the global Cartesian coordinate system O-XYZ can be converted into a new cuboidlike particle i' with its center located at the origin O' of the new Cartesian coordinate system O'-X′Y′Z′ and three semimajor axes parallel to the coordinate axes (i.e, O'X′, O'Y′, and O'Z′) as shown in Fig. 4. The shape and size of the new particle i in O'-X′Y′Z′ is identical with the cuboidlike particle i in O-XYZ and the geometrical formula of particle i' can be expressed by Eq. (23). We call this new coordinate system O'-X′Y′Z′ the local coordinate system.

$$(x_i'\ y_i'\ z_i'\ 1)^T = R_i^{-1} T_i^{-1} (x_i\ y_i\ z_i\ 1)^T, \tag{22}$$

$$\frac{|x_i'|^{2m}}{a_i^{2m}} + \frac{|y_i'|^{2m}}{b_i^{2m}} + \frac{|z_i'|^{2m}}{c_i^{2m}} = 1, \tag{23}$$

where $(x_i,\ y_i,\ z_i)$ denotes the location of points on the surface of cuboidlike particle i with respect to the global coordinated system O-XYZ, and $(x_i',\ y_i',\ z_i')$ denotes the location of corresponding points on the surface of particle i' relative to the new coordinate system O'-X′Y′Z′. T_j^{-1} and R_j^{-1} represent the inverse matrices of T_i and R_i.

$$\frac{|x_{0,j}'|^{2m}}{a_i^{2m}} + \frac{|y_{0,j}'|^{2m}}{b_i^{2m}} + \frac{|z_{0,j}'|^{2m}}{c_i^{2m}} \leqslant 1. \tag{24}$$

The center of cuboidlike particle $j[O_j\ (x_{0,j},\ y_{0,j},\ z_{0,j})]$ in O-XYZ can also be transformed into a new point $O_j'\ (x_{0,j}',$

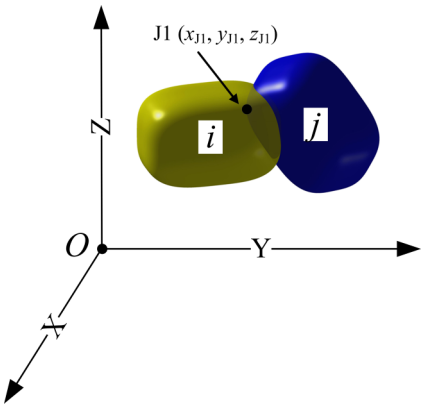

FIG. 5. Schematic diagram of accurate contact detection of two cuboidlike particles i and j.

$y'_{0,j}$, $z'_{0,j}$) in O'-X′Y′Z′. And if the new center of particle O'_j ($x'_{0,j}$, $y'_{0,j}$, $z'_{0,j}$) meets Eq. (24), we can be definitely sure that these two cuboidlike particles i and j make contact. Otherwise, a more numerically stable contact detection algorithm based on the geometric potential concept will be further utilized. Refer to the detailed description in Ref. [45] for the equation of a 3D particle $f(x, y, z) = 0$, a varying value of potential $f = f(x, y, z)$ represents a family of varying sized geometric similar particles sharing the same origin. As shown in Fig. 5, there exists a point (i.e., the black dot $J1$) on the surface of cuboidlike particle j which forms the minimum potential (i.e., the smallest f) to the other particle (i.e., the cuboidlike particle i). If this point $J1$ is inside or on the particle i [i.e., $f(x_{J1}, y_{J1}, z_{J1}) \leqslant 0$], contact must exist. Zhou *et al.* [46] utilized the above idea to develop a geometric-potential-based contact detection algorithm for egg-shaped particles and then investigated the behaviors of assemblies of egg-shaped particles at macroscopic and microscopic levels.

In this study, for the sake of convenience, the surface of a random cuboidlike particle in 3D space is simplified as a set of discrete points. The contact of two arbitrary cuboidlike particles can be determined by detecting whether the set of points which forms a surface of one particle (e.g., the particle j) is inside the other particle (e.g., the particle i). In general, the more homogeneous the distribution of the selected discrete points is, the more similar the simplified surface of a cuboidlike particle formed by those points is to the real morphology of the particle. Following Ref. [44], two ranges of discontinuous angles θ and φ are obtained by Eq. (25).

$$\theta = 0 : \frac{\pi}{n} : \pi, \tag{25a}$$

$$\varphi = 0 : \frac{\pi}{n} : 2\pi, \tag{25b}$$

where n is a random positive integer.

Substituting Eq. (25) into Eq. (10), the coordinates of distributed discrete points on the surface of one specified cuboidlike particle expressed by Eq. (1) can be obtained. Figure 6 visualizes the real morphology of a cuboidlike particle and the corresponding 3D discrete points on its surface by Eqs. (10) and (25). For an arbitrary cuboidlike particle

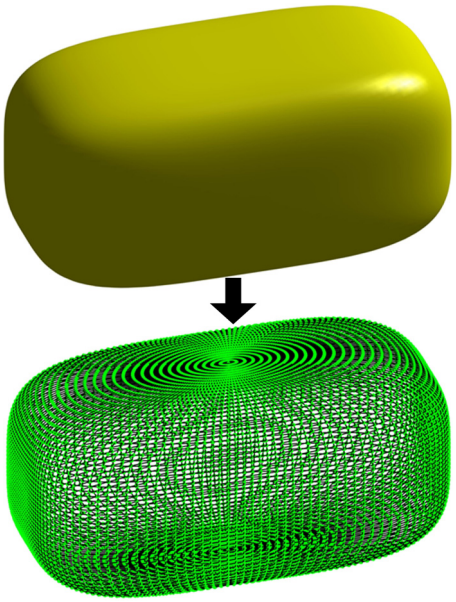

FIG. 6. Visualization of the discrete points on the surface of a cuboidlike particle with $m = 2.0$, $a = 2.0$, $b = c = 1.0$, and $n = 80$, respectively.

expressed by Eqs. (2)–(6), the coordinates of the points on the surface can be obtained easily by the linear transformation with the matrices T, R, and S.

In recent years, various methods of detecting the collision of superellipsoids have been developed. For instance, Cleary *et al.* [47] described a fast method for predicting intersuperellipsoid collision based on the Newton-Raphson scheme. By utilizing

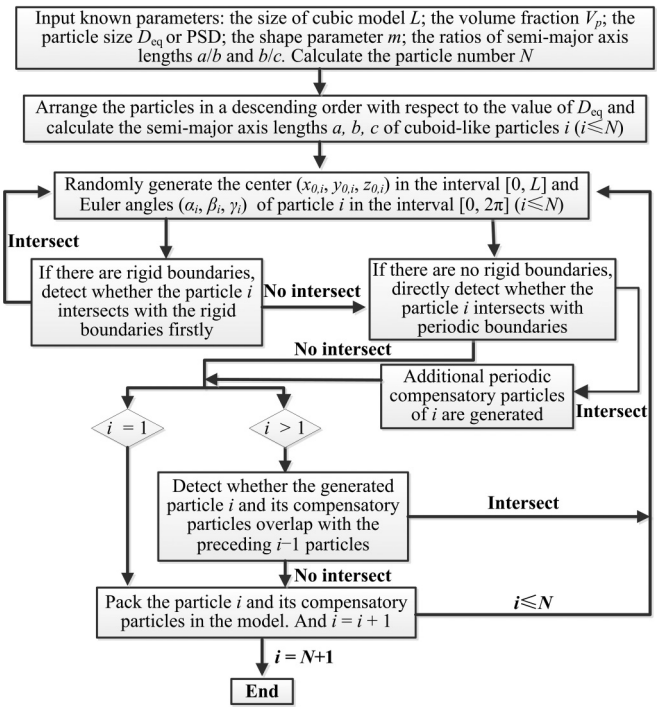

FIG. 7. Flowchart of the packing procedure of rigid cuboidlike particles in the cubic container.

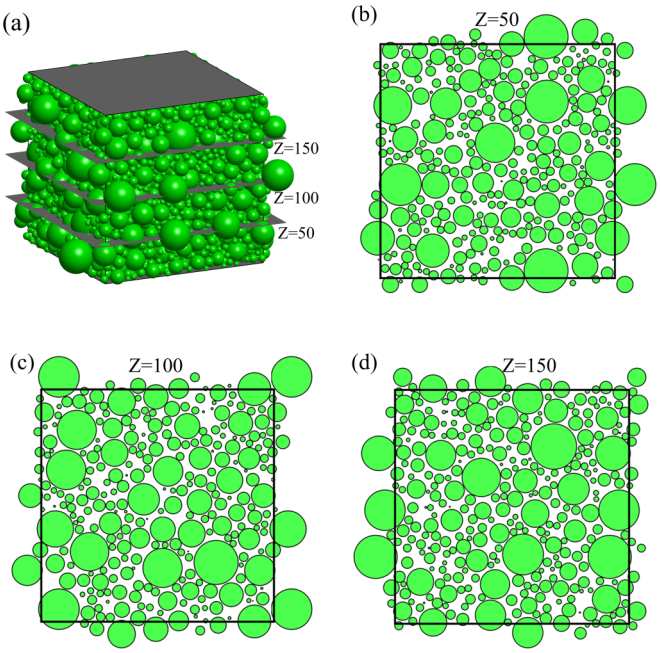

FIG. 8. Verification of the contact detection algorithm for a specified cubic packing structure of multisized rigid cuboidlike particles ($m = 1.0$ and $a = b = c$, i.e., spheres) generated by a random sequential packing approach. (a) The semiperiodic packing structure of multisized rigid particles which satisfies Fuller distribution function. (b) The intersection of the section plane $Z = 50$ and the particles. (c) The intersection of the section plane $Z = 100$ and the particles. (d) The intersections of the section plane $Z = 150$ and the particles.

the common-normal concept, Wellmann *et al.* [48] developed an efficient detection algorithm between superellipsoids and the main feature of this algorithm is to search for the contact direction instead of the contact points. Combing the common-normal concept with the discrete element method (DEM), Zhao and Zhou [49] introduced a superball-based DEM model and the effect of particle shape on the mechanical behaviors of monodisperse assemblies was investigated. Compared with these above-mentioned approaches, the characteristic of our algorithm is that the surface of an arbitrary cuboidlike particle is assumed to be composed of a set of 3D discrete points. The interparticle contact can be determined by detecting whether the points on the surface of one cuboidlike particle are inside the other one. Furthermore, combining the linear coordinate transformation with vector and matrix operation theory, the position relationship between a series of 3D discrete points and the other nonspherical particle can be quickly determined instead of detecting the iteration as described in Refs. [15,40].

C. Verification of the contact detection algorithm

In order to verify the reliability of the contact detection algorithm for cuboidlike particles, a specified cubic packing structure of multisized rigid cuboidlike particles with $m = 1.0$ and $a = b = c$ (i.e., spherical particles) is generated by means of a random sequential packing approach. The detailed packing procedure is illustrated in Fig. 7. In the particle packing structure shown in Fig. 8(a), the container is set to semiperiodic boundary conditions (i.e., both the upper and lower walls are set to rigid boundaries, and the other four walls are set to periodic boundaries), and the side length L is equal to 200. For the periodic boundaries, if the particle overlaps with the boundary planes, a periodic compensation strategy [50] will be applied. The volume fraction of rigid particles V_P in the container is selected to be 0.60 and the equivalent radius R_{eq}, which is defined as the radius of an equivalent sphere having the same volume as an arbitrary cuboidlike particle, is used by Eq. (26).

$$R_{\mathrm{eq}} = \Gamma(0.5/m)\left[\frac{abc}{2\pi\Gamma(1.5/m)m^2}\right]^{1/3}, \tag{26}$$

where R_{eq} is the radius of an equivalent sphere having the same volume as the cuboidlike particles with a, b, c, and m.

For the packing of rigid spherical particles in Fig. 8, the values of R_{eq}, a, b, and c are identical for an arbitrary particle. The Fuller distribution function [14] is employed to represent the particle size distribution (PSD) of multisized rigid particles. The maximum and minimum equivalent radii (i.e., $R_{\mathrm{eq,max}}$ and $R_{\mathrm{eq,min}}$) are, respectively, set to 3 and 20. The integer n in Eq. (25) is selected to be 80. Three section planes parallel to the rigid boundary planes (i.e., $Z = 50$, 100, and 150) are used to intercept the corresponding model structures, respectively. It can be seen from Figs. 8(b)–8(d) that no interparticle overlapping occurs in all of these slices, which indicates the reliability of our interparticle contact detection algorithm.

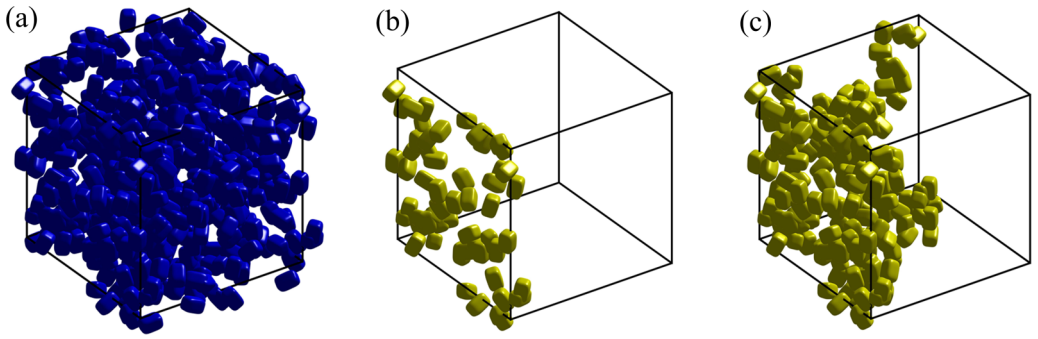

FIG. 9. The searching algorithm for percolation cluster in the congruent overlapping cuboidlike particle packing structure with periodic boundaries. (a) Realization of overlapping particle packing structure. (b) The particles overlapping with the left boundary plane. (c) Identification of a percolation cluster.

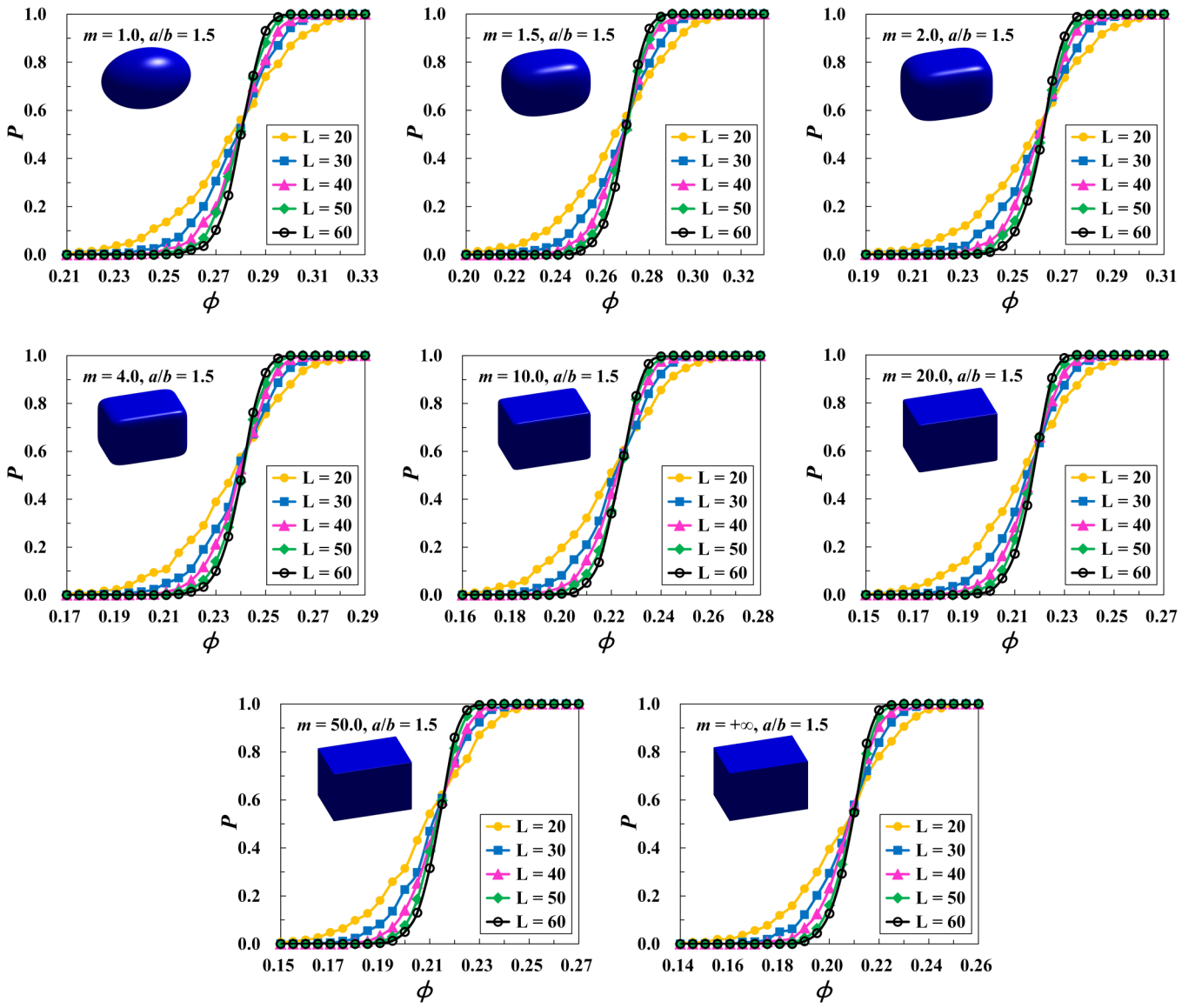

FIG. 10. Percolation probability $P(\phi, L)$ vs ϕ with $a/b = 1.5$ and different m.

D. Percolation model in particle systems

Through the combination of the model of cuboidlike particles, the contact detection algorithm, and the percolation model [35], a simple searching algorithm for percolation cluster in overlapping cuboidlike particle packing structure is presented.

As shown in Fig. 9(a), we first generate a realization of congruent overlapping cuboidlike particles with fixed particle size R_{eq}, shape parameter m, the ratio of semimajor axis length a/b (where $b = c$), and covering volume fraction ϕ in the cubic container of size L by a random sequential addition (RSA) process. The centers $(x_0,\ y_0,\ z_0)$ and Euler angles $(\alpha,\ \beta,\ \gamma)$ of particles are randomly selected in the intervals of $[0,\ L]$ and $[0,\ 2\pi]$, respectively, which means that all the particles' positions and orientations are totally uncorrelated. All the boundary planes of the container are set to be periodic, and the periodic compensation strategy [50] is applied as well. The total number of particles N is determined by Eqs. (27) and (28).

$$N = \frac{L^3 \ln(1-\phi)^{-1}}{V}, \tag{27}$$

$$V = \frac{2}{3}\frac{\Gamma^3(0.5/m)}{\Gamma(1.5/m)m^2}abc, \tag{28}$$

where V is the volume of a cuboidlike particle and can be calculated by Eq. (28), ϕ is a given covering volume fraction of particles, and L is the side length of the cubic container.

Taking the left and right planes of the cubic structure for example, search for the particles which overlap with the left plane of the container, and label them by a new color [i.e., the yellow particles in Fig. 9(b)]. Subsequently, based on the contact detection algorithm, search for the particles which overlap with the preceding particles labeled by the yellow, and label them by the same color as well. This process is iterated until there is no additional particle overlapping with

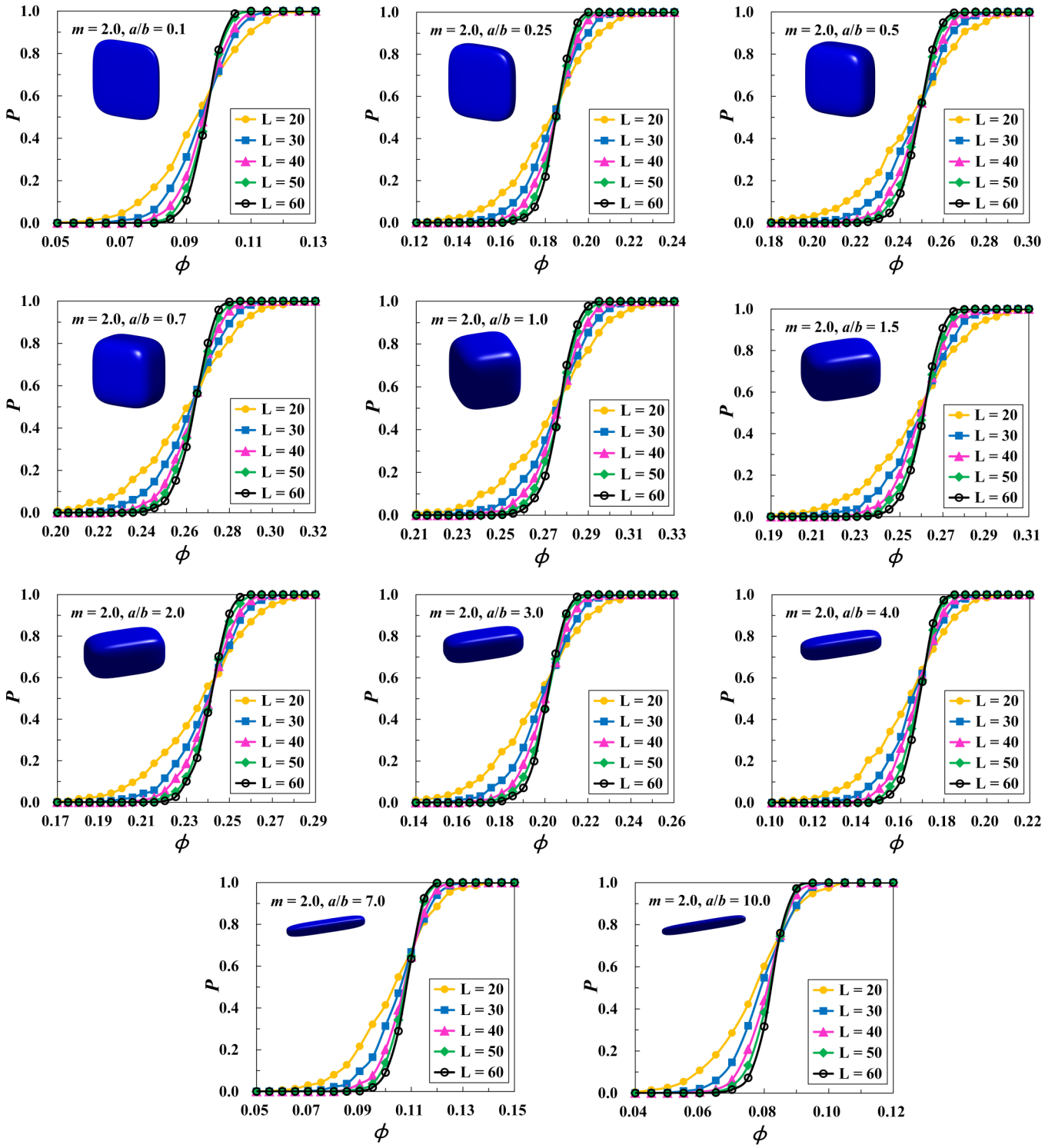

FIG. 11. Percolation probability $P(\phi, L)$ vs ϕ with $m = 2.0$ and different a/b.

the preceding particles. Finally, detect whether or not these particles denoted by new color interact with the right plane. If one intersection is found as shown in Fig. 9(c), the connected path throughout the horizontal direction of the structure is formed and the percolation is realized. Otherwise, we need to further detect the relationship between these particles and the other four planes of the container.

In the finite-size systems, the percolation occurs with a certain probability. For an overlapping particle system with given volume fraction ϕ, a large number of samples are generated and each is checked. The percolation probability P defined as the ratio of percolated samples N_p to the total samples N_t is computed by Eq. (29). If the number of total samples N_t is high enough, a reliable value of P can be

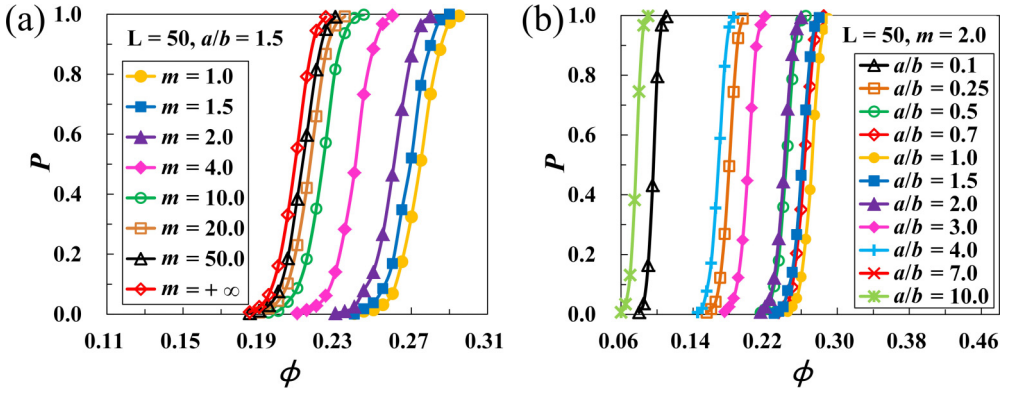

FIG. 12. Effect of cuboidlike particle shapes on the curves of P-ϕ with $L/R_{\rm eq} = 50$. (a) Effect of the parameter m. (b) Effect of the aspect ratio a/b.

obtained.

$$P = \frac{N_p}{N_t}, \tag{29}$$

where N_t is the total number of generated samples, and N_p is the number of percolated samples.

III. APPLICATIONS AND DISCUSSIONS

A. Percolation probability

A series of percolation models of congruent overlapping cuboidlike particles with different morphologies are generated in the cubic container of size L. For all the cuboidlike particles in the models, the semimajor axis length b is equal to the length c. The shape parameter m is selected to be 1.0, 1.5, 2.0, 4.0, 10.0, 20.0, 50.0, and $+\infty$, respectively. The ratio of semimajor axis lengths a/b is equal to 0.1, 0.25, 0.5, 0.7, 1.0, 1.5, 2.0, 3.0, 4.0, 7.0, and 10.0, respectively. According to the study [35], the percolation threshold possesses a universal behavior dependent only on the particle shape but not particle size for the percolation of congruent overlapping particles. Thus, the equivalent radius of particles $R_{\rm eq}$ here is fixed to be a constant 1.0 and the ratio of L to $R_{\rm eq}$ is assigned as at least 20 (i.e., $L/R_{\rm eq} \geqslant 20$). To guarantee the statistical reliability of the results, the number of total samples [i.e., N_t in Eq. (29)] is assigned as 2000 for each percolation structure based on our previous work [44].

Figures 10 and 11 illustrate the percolaton probability of finite-size cuboidlike particle packing structures P as a function of volume fraction ϕ for different m and a/b, respectively. It can be observed that the percolation probability P increases monotonically with the increasing volume fraction ϕ. All the shapes of the P-ϕ curves are very similar to the curves of Gauss error function. Besides, the ratio $L/R_{\rm eq}$ (i.e., the side length L) has remarkable impact on the curves of P-ϕ. For the percolation models with fixed m and a/b, the curve of P-ϕ becomes steeper with the increase of L from 20 to 60, and the maximum slope of the P-ϕ curve also grows as well. Predictably, as the side length of structures L approaches to infinity, the slope of the P-ϕ curve tends to infinity and the corresponding volume fraction ϕ on the horizontal axis of Figs. 10 and 11 will be a constant value. Besides, we also find from Figs. 10 and 11 that the crossing points of the P-ϕ curves are generally at different values of ϕ for different cuboidlike particles and are closely related on the positions of those obtained curves of P-ϕ.

Figure 12 displays the influence of cuboidlike particle shape (i.e., m and a/b) on the curves of P-ϕ with $L/R_{\rm eq} = 50$. It can be seen from Fig. 12 that both the shape parameter m and the ratio a/b do not significantly affect the shapes of the P-ϕ curves, and the percolation probability P in the curves of P-ϕ

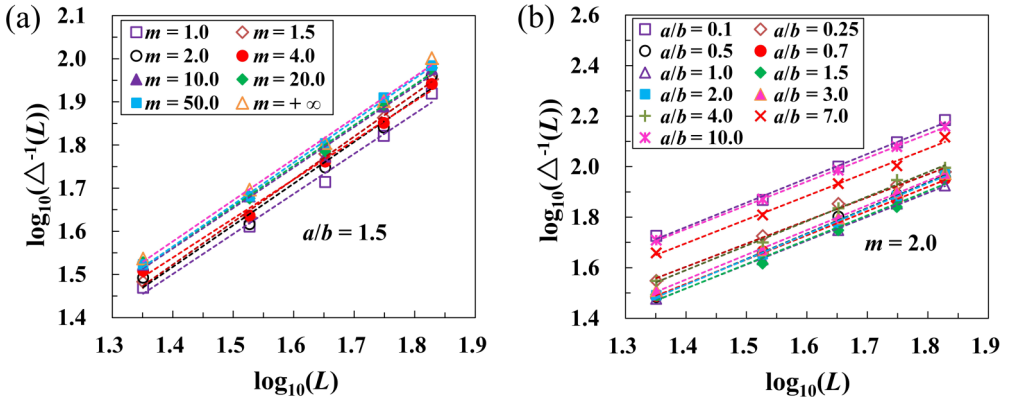

FIG. 13. The negative power of percolation transition width $\Delta^{-1}(L)$ as a function of L for different particle shapes. (a) Effect of the parameter m. (b) Effect of the aspect ratio a/b.

TABLE I. The values of critical exponent v of cuboidlike particles with different m at $a/b = 1.5$ from Fig. 13(a).

m	1.0	1.5	2.0	4.0	10.0	20.0	50.0	$+\infty$
v	1.075	1.01	1.034	1.102	1.064	1.062	1.027	1.042

increases with volume fraction ϕ. At $L/R_{eq} = 50$, all of the slopes of the P-ϕ curves with m in [1.0, $+\infty$) and a/b in [0.1, 10] remain basically invariable, but the vertical asymptotic value of the P-ϕ curve along the horizontal axis (i.e., ϕ axis) is dominated by the particle shape. By comparing the curves of P-ϕ with different m in Fig. 12(a), we can find that the P-ϕ curve shifts to a lower value of ϕ with the increasing m from 1.0 to $+\infty$. That is to say, more cuboidlike particles are interconnected at high m, and such systems percolate at lower volume fraction. Compared with the curves of P-ϕ with different a/b in Fig. 12(b), it is observed that when $0.1 \leqslant a/b \leqslant 1.0$, the P-ϕ curve translates to higher volume fraction along the horizontal axis (i.e., ϕ axis) with the increasing a/b. However, as the ratio a/b continues to increase from 1.0, the P-ϕ curve translates to lower ϕ along the horizontal axis of Fig. 12(b), which is similar to the trends of curves of P-ϕ for congruent ellipsoids [32].

B. Percolation threshold

The percolation threshold ϕ_c in the infinite space characterizes the critical state of emergence of the spanning cluster. To obtain the corresponding percolation threshold for different systems, researchers have developed various numerical methods and many good research achievements have been accumulated so far. For instance, Lorenz and Ziff [51] used extensive Monte Carlo simulations to evaluate the excess number of clusters and the crossing probability function for 3D percolation on the simple cubic, face-centered cubic, and body-centered cubic lattices. The results revealed that the excess number of clusters per unit length is a universal quantity with a value of 0.412 and the critical crossing probability followed a universal exponential decay. In the literature [52], Newman and Ziff described an efficient algorithm for studying site or bond percolation on any lattice. The algorithm can be used to measure an observable quantity in a percolation system for all values of the site or bond occupation probability from 0 to 1 in an amount of time that scales linearly with the size of the system. For the continuum percolation model of particles, a comprehensive finite-sized scaling analysis technique was adopted successively by different researchers [26,35,44] to explore the effect of particle shape on the percolation behavior of particle packing systems in a periodic cubic domain and the generalized approximations for the threshold ϕ_c were obtained. In our study, the percolation threshold ϕ_c is also represented by a critical volume fraction of overlapping particles. In order to derive the percolation threshold ϕ_c for the cuboidlike particle packing systems from the percolation probability P and formulize the influence of cuboidlike particle morphologies on the value of ϕ_c, the simple finite-size scaling technology as described in Ref. [26] is utilized here without regard to the small deviation caused by the assumptions in this method.

According to the implemented process of the finite-size scaling method [32,35], a Gauss error function, as Eq. (30), is used to fit the obtained P-ϕ curves in the simulation (e.g., the curves in Fig. 10 and 11). Then, the local percolation threshold $\phi_c(L)$ and the percolation transition width $\Delta(L)$ can be derived.

$$P(\phi, L) = \frac{1}{2}\left\{1 + \mathrm{erf}\left[\frac{\phi - \phi_c(L)}{\Delta(L)}\right]\right\}, \tag{30}$$

where $\phi_c(L)$ is the local percolation threshold for a system of size L. The condition $P(\phi, L) = 0.5$ is used to determine the critical value of $\phi_c(L)$ for the finite system. $\Delta(L)$ denotes the width of the percolation transition in the finite-size structures.

By fitting the curves in Figs. 10 and 11, Fig. 13 shows the log-log plot of $\Delta^{-1}(L)$ against L for different m and a/b, respectively. It can be seen that $\Delta^{-1}(L)$ is a quantity clearly depending on the system size L. When the values of m and a/b are fixed, all the values of $\log_{10}[\Delta^{-1}(L)]$ increase linearly with the increase of $\log_{10}(L)$. Additionally, all the curves of $\log_{10}[\Delta^{-1}(L)]$–$\log_{10}(L)$ are approximately parallel to one another at the same m (or a/b). In the literature [26,32,35], $\Delta^{-1}(L)$ is described as a function of system size L via a correlation-length critical exponent v. According to the scaling relation between $\Delta(L)$ and L as expressed by Eq. (31), the corresponding exponent v can be obtained from Fig. 13 where their values are equal to the slopes of these lines. In Tables I and II, the specified values of the exponent v from Figs. 13(a) and 13(b) are listed in detail, respectively. It can be shown that the critical exponent v for a cuboidlike particle with different shapes in our study is not a constant. All of the corresponding values of v obtained fluctuate around 1.0 which is slightly different from the results ($v \approx 0.876$) in the literature [53,54].

$$\Delta^{-1}(L) \propto L^{1/v}, \tag{31}$$

where v is a correlation-length critical exponent.

$$\phi_c(L) - \phi_c \propto L^{-1/v}. \tag{32}$$

After deriving $\phi_c(L)$ and v, the global percolation threshold ϕ_c can be subsequently estimated by Eq. (32). Figures 14(a) and 14(b) illustrate the variations of the local percolation threshold $\phi_c(L)$ as a function of $L^{-1/v}$ for the conditions of $a/b = 1.5$ and $m = 2.0$, respectively. The interception of each curve of $\phi_c(L)$-$L^{-1/v}$ the with y axis is the corresponding ϕ_c for infinite-size systems. Taking the simulated results with $m = 1.0$ and $a/b = 1.0$ as an example, the percolation threshold $\phi_c = 0.2896 \pm 0.0004$ is obtained from a linear fitting to the simulated data. The value of ϕ_c is basically consistent with the simulated results by Rintoul and Torquato

TABLE II. The values of critical exponent v of cuboidlike particles with different a/b at $m = 2.0$ from Fig. 13(b).

a/b	0.1	0.25	0.5	0.7	1.0	1.5	2.0	3.0	4.0	7.0	10.0
v	1.037	1.091	0.992	1.041	1.052	1.034	0.997	1.019	1.030	1.027	1.062

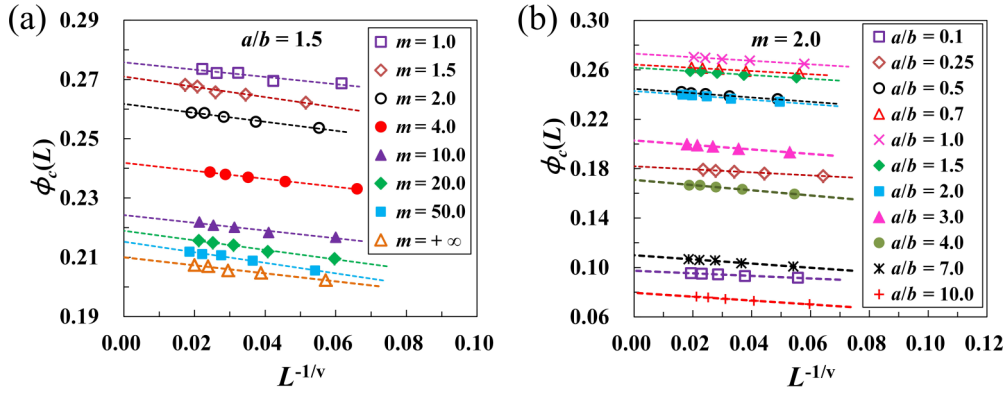

FIG. 14. The local percolation threshold $\phi_c(L)$ as a function of $L^{-1/\nu}$ for different m and a/b. (a) Effect of the parameter m. (a) Effect of the aspect ratio a/b.

($\phi_c = 0.2895 \pm 0.0005$) [26], Lorenz and Ziff ($\phi_c = 0.289573 \pm 0.000002$) [27], Garboczi *et al.* ($\phi_c = 0.2854$) [31], and Xu *et al.* ($\phi_c = 0.2896 \pm 0.0007$) [35]. In Table III, we list a series of the numerically simulated values of ϕ_c we obtain by the above approach.

Figure 15 visualizes the derived percolation threshold ϕ_c of congruent overlapping cuboidlike particles with m in [1.0, $+\infty$) and a/b in [0.1, 10.0], respectively, where the two black solid lines in Fig. 15(b) separately correspond to the values of ϕ_c for the conditions of $m = 2.0$ and $a/b = 1.5$. It is found that ϕ_c is a heavily m- and a/b-dependent quantity, which shows different changing trends with the variation of m and a/b, respectively. As depicted in Fig. 15, at the same m, the percolation threshold ϕ_c generally shows a first increasing and then decreasing trend with the increasing a/b from 0.1 to 10.0, and the maximum threshold is obtained at $a/b = 1.0$ (i.e., ellipsoids), but the changing degree of ϕ_c is closely related to the specified value of m.

When the ratio a/b is held constant, the impact of m on the percolation threshold ϕ_c is slightly different with the variation of a/b from 0.1 to 10.0. In Fig. 15, when the value of a/b approaches 1.0, the global percolation threshold ϕ_c of overlapping cuboidlike particles decreases with the increasing m from 1.0 to $+\infty$. Meanwhile, the impact degree of m slows down with the increasing m and turns to be a stable value. However, as the ratio a/b moves to both sides from 1.0, the dependence of ϕ_c on the shape parameter m is gradually weakened. The percolation threshold ϕ_c shows a first increasing and then decreasing trend with the increasing m, which is very different with the variation of ϕ_c at $a/b = 1.0$. When the ratio a/b is large (e.g., $a/b = 10.0$) or small (e.g., $a/b = 0.1$) enough, the influence of m on the value of ϕ_c can be neglected. Overall, the influence of the ratio a/b on the percolation threshold ϕ_c is greater than that of the parameter m, and the percolation threshold ϕ_c possesses a maximum value at $a/b = 1.0$ and $m = 1.0$, which indicates that the systems of congruent overlapping spheres are more difficult to percolate than other cuboidlike particles. Such conclusion has similarities with the results for congruent ellipsoids [31] and spherocylinders [35].

C. An analytical approximation

Based on the simulated results in Fig. 15, we propose an analytical approximation for percolation threshold ϕ_c of congruent overlapping cuboidlike particles [i.e., Eq. (33)], in which the exponent is closely related to the dimensionless excluded volume V_{dex}, the shape parameter m, and the aspect ratio a/b.

$$\psi_c = 1 - e^{-G/V_{dex}}, \tag{33}$$

TABLE III. The statistically simulated values of percolation threshold ϕ_c of cuboidlike particles with specified m and a/b.

a/b \ m	1.0	1.5	2.0	4.0	10.0	20.0	50.0	$+\infty$
0.1	0.0895 ± 0.0004	0.0957 ± 0.0002	0.0973 ± 0.0002	0.0950 ± 0.0004	0.0906 ± 0.0004	0.0899 ± 0.0001	0.0883 ± 0.0003	0.0875 ± 0.0002
0.25	0.1783 ± 0.0003	0.1833 ± 0.0001	0.1819 ± 0.0002	0.1712 ± 0.0002	0.1613 ± 0.0003	0.1576 ± 0.0003	0.1551 ± 0.0002	0.1522 ± 0.0002
0.5	0.2537 ± 0.0002	0.2518 ± 0.0005	0.2447 ± 0.0003	0.2268 ± 0.0005	0.2111 ± 0.0003	0.2062 ± 0.0001	0.2022 ± 0.0002	0.1985 ± 0.0008
0.7	0.2784 ± 0.0005	0.2739 ± 0.0004	0.2643 ± 0.0003	0.2441 ± 0.0002	0.2268 ± 0.0001	0.2207 ± 0.0003	0.2167 ± 0.0002	0.2120 ± 0.0002
1.0	0.2896 ± 0.0004	0.2819 ± 0.0002	0.2729 ± 0.0003	0.2513 ± 0.0003	0.2335 ± 0.0003	0.2262 ± 0.0002	0.2220 ± 0.0003	0.2174 ± 0.0004
1.5	0.2757 ± 0.0007	0.2709 ± 0.0004	0.2617 ± 0.0003	0.2419 ± 0.0002	0.2242 ± 0.0004	0.2189 ± 0.0003	0.2152 ± 0.0002	0.2100 ± 0.0003
2.0	0.2537 ± 0.0005	0.2503 ± 0.0002	0.2428 ± 0.0002	0.2258 ± 0.0001	0.2106 ± 0.0003	0.2041 ± 0.0003	0.2008 ± 0.0006	0.1962 ± 0.0004
3.0	0.2033 ± 0.0004	0.2060 ± 0.0001	0.2028 ± 0.0002	0.1916 ± 0.0004	0.1794 ± 0.0006	0.1746 ± 0.0001	0.1725 ± 0.0002	0.1691 ± 0.0002
4.0	0.1666 ± 0.0002	0.1745 ± 0.0006	0.1708 ± 0.0002	0.1628 ± 0.0003	0.1538 ± 0.0003	0.1507 ± 0.0001	0.1479 ± 0.0005	0.1442 ± 0.0002
7.0	0.1022 ± 0.0003	0.1100 ± 0.0003	0.1099 ± 0.0003	0.1080 ± 0.0004	0.1033 ± 0.0002	0.1014 ± 0.0003	0.1009 ± 0.0003	0.0977 ± 0.0002
10.0	0.0724 ± 0.0002	0.0781 ± 0.0003	0.0796 ± 0.0002	0.0778 ± 0.0003	0.0768 ± 0.0001	0.0753 ± 0.0002	0.0749 ± 0.0002	0.0728 ± 0.0004

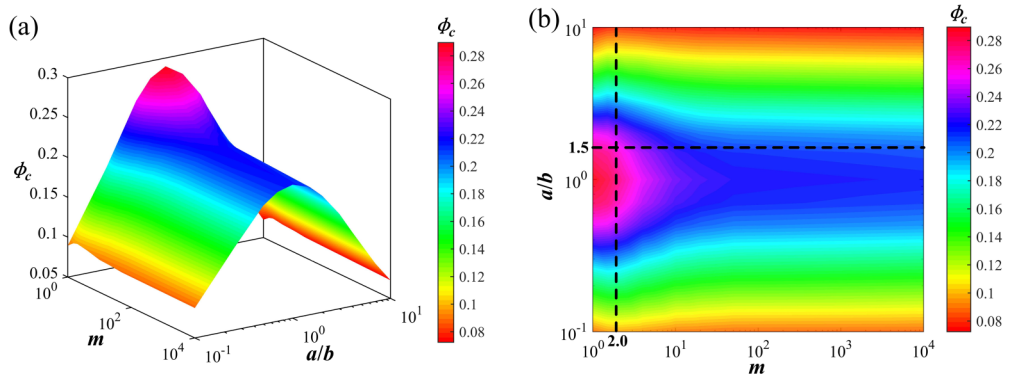

FIG. 15. Visualization of the global percolation threshold ϕ_c of congruent overlapping cuboidlike particles. (a) The 3D graphic model. (b) Top-down graph.

where the numerator G in the exponent is a coefficient related to the shapes of cuboidlike particles (i.e., m and a/b), and V_{dex} is the dimensionless excluded volume of a cuboidlike particle and can be calculated via Eq. (34).

$$V_{dex} = \frac{2V + 2S\bar{R}}{V} = 2 + \frac{2S\bar{R}}{V}, \tag{34}$$

where V, S, and $\bar{R}$ are the volume, the surface area, and the mean curvature radius of a cuboidlike particle with arbitrary shapes, respectively.

As mentioned in Ref. [22], the values of S and $\bar{R}$ for a cuboidlike particle can be obtained via the following two general formulas [i.e., Eqs. (35) and (36)], respectively.

$$S = 8\int_0^{\pi/2} d\theta \int_0^{\pi/2} d\varphi |\mathbf{x}_\theta \times \mathbf{x}_\varphi|, \tag{35}$$

$$\begin{aligned}\bar{R} = \frac{8}{4\pi}\int_0^{\pi/2} d\theta \int_0^{\pi/2} d\varphi \{&(\mathbf{x}_\theta \cdot \mathbf{x}_\theta)[(\mathbf{x}_\theta \times \mathbf{x}_\varphi)\cdot \mathbf{x}_{\varphi\varphi}] \\ &+ (\mathbf{x}_\varphi \cdot \mathbf{x}_\varphi)[(\mathbf{x}_\theta \times \mathbf{x}_\varphi)\cdot \mathbf{x}_{\theta\theta}] \\ &- 2(\mathbf{x}_\theta \cdot \mathbf{x}_\varphi)[(\mathbf{x}_\theta \times \mathbf{x}_\theta)\cdot \mathbf{x}_{\theta\varphi}]\} \\ &\times [2(\mathbf{x}_\theta \cdot \mathbf{x}_\theta)(\mathbf{x}_\varphi \cdot \mathbf{x}_\varphi) - 2(\mathbf{x}_\theta \cdot \mathbf{x}_\varphi)^2]^{-1},\end{aligned} \tag{36}$$

where the factor of 8 comes from integrating only over the quadrant due to symmetry. $\mathbf{x}$ represents a vector from the origin to the surface at a given θ and φ. $\mathbf{x}_\theta$ and $\mathbf{x}_\varphi$ are the first partial derivatives of the vector $\mathbf{x}$, and $\mathbf{x}_{\theta\theta}$, $\mathbf{x}_{\varphi\varphi}$, and $\mathbf{x}_{\theta\varphi}$ are the second partial derivatives of the vector $\mathbf{x}$. The detailed expressions of the vector $\mathbf{x}$ and its partial derivatives for cuboidlike particles in the study are shown in Appendix.

For the prolate spheroids ($b = c,\ a \geqslant b$),

$$e^2 = 1 - (b/a)^2, \tag{37a}$$

$$V_{dex} = 2 + \frac{3}{2}\left(1 + \frac{a}{be}\sin^{-1}e\right)\left(1 + \frac{b^2}{a^2 e}\tanh^{-1}e\right). \tag{37b}$$

For the oblate spheroids ($b = c,\ a \leqslant b$),

$$e^2 = 1 - (a/b)^2, \tag{38a}$$

$$V_{dex} = 2 + \frac{3}{2}\left(1 + \frac{a^2}{b^2 e}\tanh^{-1}e\right)\left(1 + \frac{b}{ae}\sin^{-1}e\right). \tag{38b}$$

After deriving the volume, the surface area, and the mean curvature radius of a cuboidlike particle with arbitrary shapes by Eqs. (28), (35), and (36), the dimensionless excluded volume V_{dex} can be subsequently calculated from the quantitative relation [i.e., Eq. (34)], as listed in Table IV. Figure 16 presents the comparison of the statistical results of V_{dex} in our study with the corresponding values obtained by the analytical formula of dimensionless excluded volume of spheroids [i.e., Eqs. (37) and (38)] in Ref. [55], and the excellent agreement can be concluded. Figure 17 shows the 3D variation of the dimensionless excluded volume V_{dex} of a cuboidlike particle V_{dex} with m in $[1.0,\ +\infty)$ and a/b in $[0.1, 10.0]$. It is observed

TABLE IV. The statistical values of dimensionless excluded volumes V_{dex} of cuboidlike particles with specified m and a/b.

a/b \ m	1.0	1.5	2.0	4.0	10.0	20.0	50.0	$+\infty$
0.1	26.387	24.438	24.162	24.734	25.898	26.485	27.032	27.203
0.25	12.956	12.620	12.790	13.595	14.549	14.986	15.286	15.491
0.5	9.077	9.191	9.478	10.313	11.176	11.557	11.816	11.992
0.7	8.275	8.478	8.786	9.623	10.463	10.831	11.080	11.264
1.0	8.000	8.233	8.548	9.384	10.216	10.580	10.825	11.000
1.5	8.357	8.551	8.857	9.693	10.536	10.905	11.155	11.333
2.0	9.077	9.190	9.476	10.312	11.176	11.557	11.815	11.992
3.0	10.907	10.809	11.041	11.867	12.778	13.187	13.466	13.658
4.0	12.956	12.615	12.782	13.588	14.545	14.983	15.284	15.498
7.0	19.546	18.419	18.361	19.066	20.142	20.661	21.033	21.285
10.0	26.381	24.440	24.138	24.709	25.882	26.475	26.878	27.225

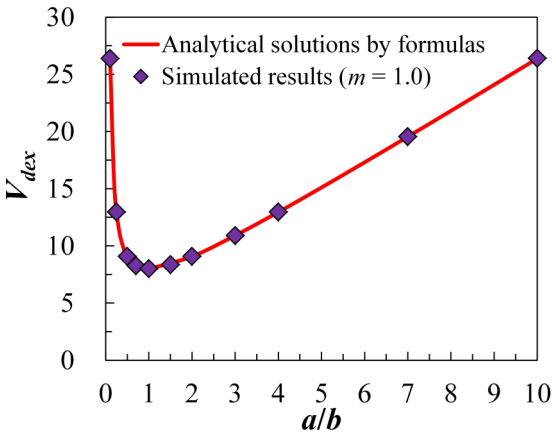

FIG. 16. Comparison of the simulated values of V_{dex} at $m = 1.0$ in the study with the analytical results for spheroids by Eqs. (37) and (38).

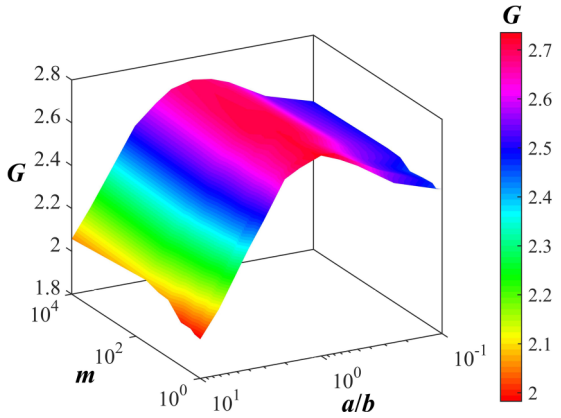

FIG. 18. Variation of the coefficient G in Eq. (33) with different m and a/b by numerical calculation.

that the value of V_{dex} is closely related to both m and a/b, and the minimum value $V_{dex,\min} = 8.000$ is obtained at $m = 1.0$ and $a/b = 1.0$.

Substituting the simulated results of ϕ_c in Fig. 15 and V_{dex} in Fig. 17 into Eq. (33), the coefficient G in the exponent can be determined by numerical calculation. From the trend of the curved surface in Fig. 18, we can find that G is a heavily shape-dependent quantity. By comparison, when a/b is held constant, the variation of G with the increase of m is very small, which can be neglected. For the sake of simplicity, it is assumed that the coefficient G in Eq. (33) is only a function of a/b [i.e., $G(a/b)$]. By fitting the curved surface in Fig. 18, the function of $G(a/b)$ can be approximately expressed by Eq. (39).

$$G(a/b) = 0.012\ln^4(a/b) - 0.015\ln^3(a/b) - 0.157\ln^2(a/b) - 0.024\ln(a/b) + 2.724. \quad (39)$$

In the literature [36,55], Torquato and Jiao characterized the percolation threshold as the critical reduced density η_c and obtained the rigorous theoretical bounds for the percolation threshold of congruent overlapping convex hyperparticles. According to the relation between the critical density η_c and the critical volume fraction (i.e., the threshold ϕ_c) described by Eq. (40) [56], Xu *et al.* [35] rewrote the rigorous bounds for the critical volume fraction of monodisperse soft convex particles in 3D space, and the lower and upper bounds can be expressed by Eqs. (41a) and (41b), respectively.

$$\phi_c = 1 - e^{-\eta_c}, \quad (40)$$

where η_c is the critical reduced density of overlapping particles.

$$\phi_{c,\text{lower}} = 1 - e^{-1/V_{dex}}, \quad (41a)$$

$$\phi_{c,\text{upper}} = 1 - e^{-2.7344/V_{dex}}. \quad (41b)$$

As described by Eqs. (41a) and (41b), it can be seen that the numerators in the exponent for the lower and upper bounds are separately a fixed constant (i.e., 1 and 2.7344). In our study, the coefficient G is considered to be a function of a/b, and the maximum and minimum values of G for congruent overlapping cuboidlike particles with m in $[1.0, +\infty)$ and a/b in [0.1, 10.0] are equal to 2.724 and 1.99, respectively. All of the results obtained by Eq. (39) lie within the rigorous bounds (i.e., 1.0 and 2.7344). By comparison, we also find all the obtained values of G are relatively close to the upper bound. The closer the ratio a/b is to 1.0, the larger the numerical value of G would be. In Fig. 19, we further compare the present result of ϕ_c with the upper and lower bounds for the percolation threshold of overlapping particles obtained by Eq. (41). It can be clearly seen that our analytical approximations are in excellent agreement

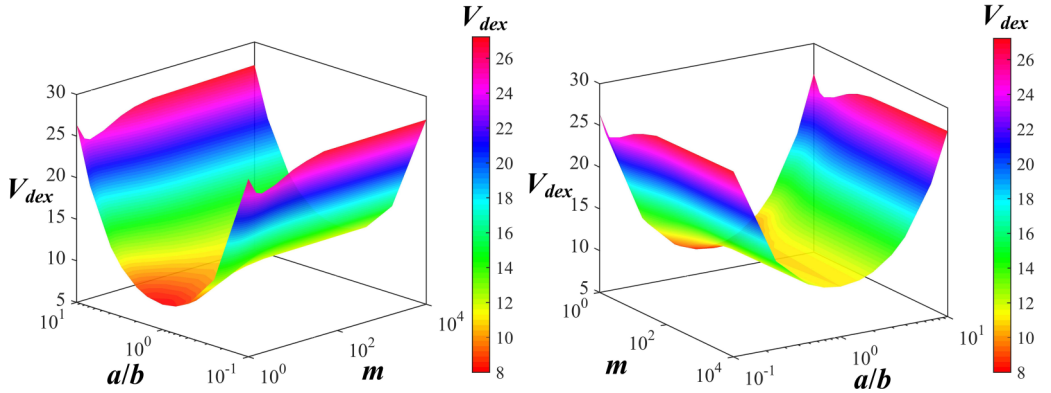

FIG. 17. 3D visualizations of the dimensionless excluded volume of a cuboidlike particle V_{dex} with different m and a/b from different perspectives.

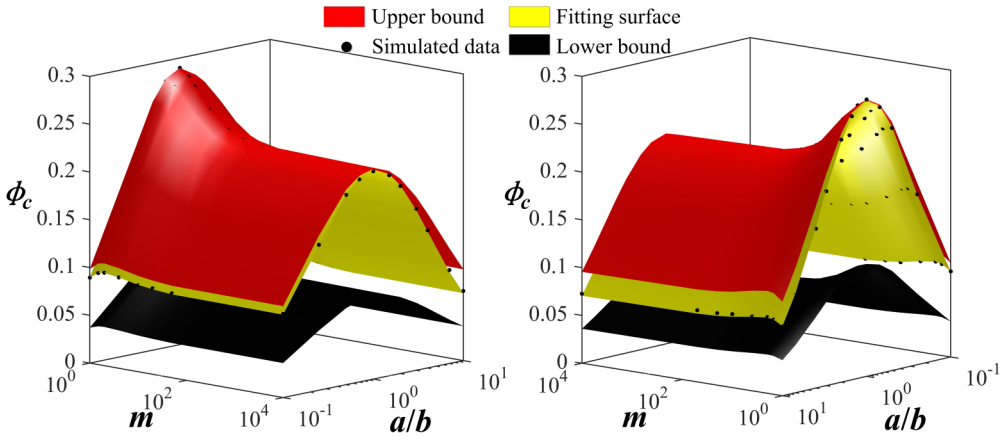

FIG. 19. Visualizations of the comparisons of the present results of ϕ_c with the rigorous bounds by Eq. (41) from two different perspectives.

with the simulated results. All of our results for overlapping cuboidlike particles lie within the rigorous upper and lower bounds and are close to the upper bound, which indicate that the present simulations and the finite-size scaling analysis can be used to generate good estimates of the percolation threshold ϕ_c for a wide range of a/b and m.

We compare the percolation threshold ϕ_c of overlapping cuboidlike particles by the derived approximation [i.e., Eq. (33)] with the numerical and simulated results in Refs. [31,32] and the results in Ref. [44]. Figure 20(a) shows the variation trend of the global percolation threshold of congruent overlapping spheroids with the increasing a/b from 0.1 to 10.0. It is shown that the analytical solutions of ϕ_c with $m = 1.0$ are generally slightly lower than the numerical results of congruent spheroids by Garboczi *et al.* [31]. They are in conformity with the corresponding data by Yi and Sastry [32]. In Fig. 20(b), the simulated threshold of overlapping superballs obtained in Ref. [44] is employed to compare with our approximations for the condition of $a/b = 1.0$, and excellent agreement is also observed. All these comparisons in Fig. 20 indicate that the analytical formula we derived can be used to provide good estimates of the percolation threshold ϕ_c of convex particles with a great number of shapes.

It is known from the study by Lorenz and Ziff [51] that for the cubic structures with periodic boundaries, the threshold can also be obtained at the condition of the crossing probability $P = 0.573$. This crossing probability is a universal property and can be applied for all the systems of the same boundary geometry. By using the above criterion, we obtained the corresponding values of ϕ directly at $P = 0.573$ and $L = 60$ through the crossing curves of P-ϕ in Figs. 10 and 11. Figures 21(a) and 21(b) clearly show the comparison of the numerical results of ϕ_c by the scaling method with the values of ϕ corresponding to $P = 0.573$ and $L = 60$. It can be found that the obtained values of ϕ are also in excellent agreement with ϕ_c.

IV. CONCLUSIONS

In this paper, we have presented a geometrical model of the cuboidlike particles with arbitrary positions, sizes, and orientations, and developed a numerical contact detection algorithm for these nonspherical particles. The reliability of this algorithm is verified by combining the packing structure of multisized rigid spheres with the section analysis technology. Using the model of cuboidlike particles, the contact detection algorithm, and the random sequential packing method, a series of percolation models of congruent overlapping cuboidlike particles in the cubic container with periodic boundaries is generated, and the influence of particle shapes on the percolation of randomly orientated cuboidlike particles is studied via percolation theory. The percolation transition width ΔL, correlation-length critical exponent ν, and global percolation

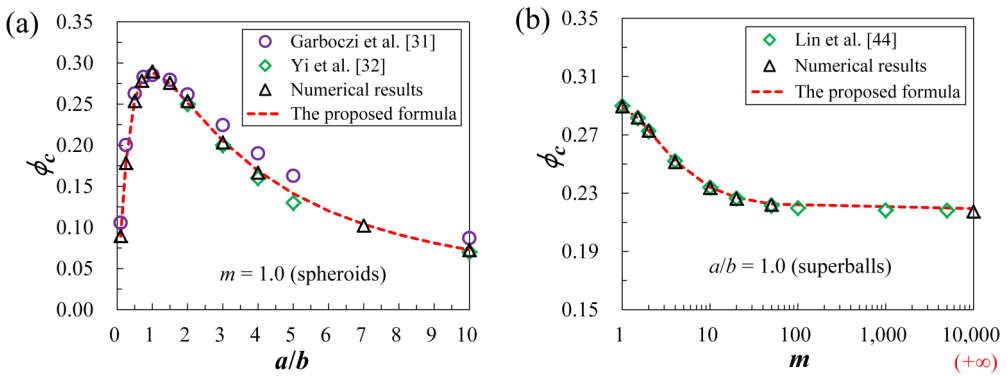

FIG. 20. Comparisons of the proposed approximation for ϕ_c with (a) the results in Refs. [31,32], and with (b) the results in Ref. [44].

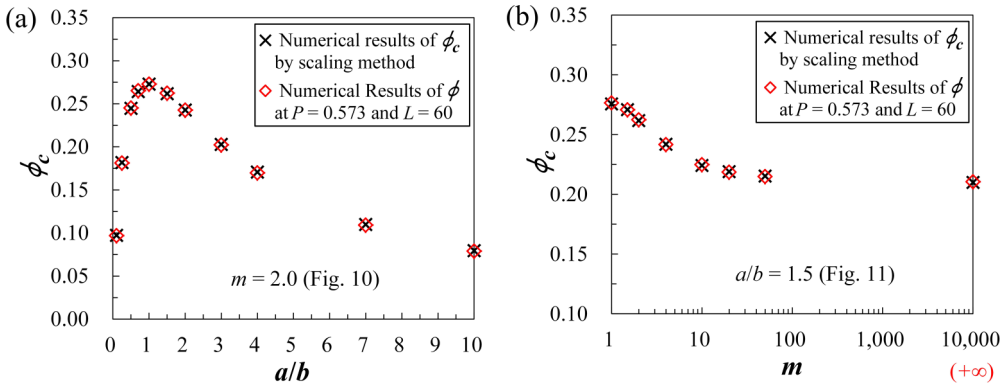

FIG. 21. Comparisons of the numerical results of ϕ_c by the scaling method with the direct values of ϕ at $P = 0.573$ and $L = 60$ for (a) the curves of P-ϕ in Fig. 10 and (b) the curves of P-ϕ in Fig. 11.

threshold ϕ_c are determined successively by a finite-size scaling analysis. Additionally, an analytical formula for ϕ_c with an exponent depending on the characteristics of cuboidlike particles (i.e., the shape parameter m and the aspect ratio a/b) is proposed by combining with the dimensionless excluded-volume approximation V_{dex}, and its reliability is verified by comparing with the results in the literature.

From the study, we can find that the percolation threshold ϕ_c is a heavily shape-dependent quantity for the cuboidlike particles. For the given shape parameters of particles here (i.e., m and a/b), the value of ϕ_c shows different changing trends with the increase of m and a/b, respectively. For a constant m in $[1.0, +\infty)$, ϕ_c generally shows a first increasing and then decreasing trend with the increasing a/b from 0.1 to 10.0, and the maximum value is obtained at $a/b = 1.0$. However, for a constant a/b in [0.1, 10.0], the impact of shape parameter m on the percolation threshold ϕ_c is slightly different, which is related to the specified value of a/b. By comparison, the influence of the ratio a/b on the percolation threshold is greater than that of the parameter m. Of all the cuboidlike particles, the maximum value $\phi_{c,\max}$ is obtained when the morphology of the cuboidlike particle becomes spherical (i.e., $m = 1.0$ and $a/b = 1.0$). The analytical approximation we derived [i.e., Eq. (33)] can be used to predict the percolation threshold ϕ_c of cuboidlike particles with a wide range of m from 1.0 to $+\infty$ and a/b from 0.1 to 10.0. It is hoped that this study can provide good guidance for the development of percolation theory and composite materials design.

In the study, the slight difference between the simulated results we obtained and the results in the literature is shown. One reason may be that the scaling technique of deriving ϕ_c we used is a relatively rough approach, in which there are some approximations: (1) the crossing function of the P-ϕ curves is considered as the derivative of the error function, which is not precise theoretically. (2) The value of $\phi_c(L)$ is obtained at the crossing probability $P = 0.5$, which is not the best estimate. While the procedure we adopted is valid and gives correct results when L goes to infinity, the convergence may be slower. Other ways may be further explored to derive the threshold ϕ_c in our future work.

ACKNOWLEDGMENTS

J.J.L. and H.S.C. gratefully acknowledge the financial support from Ministry of Science and Technology of China "973 plan" via Grant No. 2015CB655102 and National Nature Science Foundation of China via Grant No. 51461135001. W.X.X. acknowledges the financial support from National Natural Science Foundation of China via Grant No. 11772120 and Jiangsu Province National Science Foundation via Grant No. BK20170096. In addition, the authors also appreciate the help from Debra J. Audus in National Institute of Standards and Technology, Gaithersburg, MD, USA.

APPENDIX: DETAILED EXPRESSIONS OF THE VECTOR x AND ITS PARTIAL DERIVATIVES

For a cuboidlike particle described by Eq. (1), the symbol $\mathbf{x}$ represents a vector from the origin to the surface of the particle at a given θ and φ. According to Eq. (10), $\mathbf{x}$ can be expressed by Eqs. (A1)–(A3).

$$\mathbf{x} = [r(\theta,\varphi)\sin\theta\cos\varphi, r(\theta,\varphi)\sin\theta\sin\varphi, r(\theta,\varphi)\cos\theta], \tag{A1}$$

$$r(\theta,\varphi) = abcf(\theta,\varphi)^{-1/2m}, \tag{A2}$$

$$f(\theta,\varphi) = b^{2m}c^{2m}\sin\theta^{2m}\cos\varphi^{2m} + a^{2m}c^{2m}\sin\theta^{2m}\sin\varphi^{2m} + a^{2m}b^{2m}\cos\theta^{2m}. \tag{A3}$$

The first and second partial derivatives of the vector $\mathbf{x}$ (i.e., $\mathbf{x}_\theta$, $\mathbf{x}_\varphi$, $\mathbf{x}_{\theta\theta}$, $\mathbf{x}_{\varphi\varphi}$, and $\mathbf{x}_{\theta\varphi}$) are expressed by Eqs. (A4)–(A18).

$$\mathbf{x}_\theta = [\cos\varphi(r_\theta\sin\theta + r\cos\theta), \sin\varphi(r_\theta\sin\theta + r\cos\theta), r_\theta\cos\theta - r\sin\theta], \tag{A4}$$

$$\mathbf{x}_\varphi = [\sin\theta(r_\varphi\cos\varphi - r\sin\varphi), \sin\theta(r_\varphi\sin\varphi + r\cos\varphi), r_\varphi\cos\theta], \tag{A5}$$

$$\mathbf{x}_{\theta\theta} = \begin{bmatrix} \cos\varphi(r_{\theta\theta}\sin\theta + 2r_\theta\cos\theta - r\sin\theta) \\ \sin\varphi(r_{\theta\theta}\sin\theta + 2r_\theta\cos\theta - r\sin\theta) \\ r_{\theta\theta}\cos\theta - 2r_\theta\sin\theta - r\cos\theta \end{bmatrix}, \tag{A6}$$

$$\mathbf{x}_{\varphi\varphi} = \begin{bmatrix} \sin\theta(r_{\varphi\varphi}\cos\varphi - 2r_\varphi\sin\varphi - r\cos\varphi) \\ \sin\theta(r_{\varphi\varphi}\sin\varphi + 2r_\varphi\cos\varphi - r\sin\varphi) \\ r_{\varphi\varphi}\cos\theta \end{bmatrix}, \tag{A7}$$

$$\mathbf{x}_{\theta\varphi} = \begin{bmatrix} -\sin\varphi(r_\theta\sin\theta + r\cos\theta) + \cos\varphi(r_{\theta\varphi}\sin\theta + r_\varphi\cos\theta) \\ \cos\varphi(r_\theta\sin\theta + r\cos\theta) + \sin\varphi(r_{\theta\varphi}\sin\theta + r_\varphi\cos\theta) \\ r_{\theta\varphi}\cos\theta - r_\varphi\sin\theta \end{bmatrix}, \tag{A8}$$

$$r_\theta(\theta,\varphi) = \frac{-abc}{2m} f^{-1/(2m)-1} f_\theta, \tag{A9}$$

$$r_\varphi(\theta,\varphi) = \frac{-abc}{2m} f^{-1/(2m)-1} f_\varphi, \tag{A10}$$

$$r_{\theta\theta}(\theta,\varphi) = \frac{-abc}{2m} f^{-1/(2m)-2}\left[\left(\frac{-1}{2m}-1\right) f_\theta^2 + f f_{\theta\theta}\right], \tag{A11}$$

$$r_{\varphi\varphi}(\theta,\varphi) = \frac{-abc}{2m} f^{-1/(2m)-2}\left[\left(\frac{-1}{2m}-1\right) f_\varphi^2 + f f_{\varphi\varphi}\right], \tag{A12}$$

$$r_{\theta\varphi}(\theta,\varphi) = \frac{-abc}{2m} f^{-1/(2m)-2}\left[\left(\frac{-1}{2m}-1\right) f_\theta f_\varphi + f f_{\theta\varphi}\right], \tag{A13}$$

$$f_\theta(\theta,\varphi) = 2m[\sin\theta^{2m-1}\cos\theta(b^{2m}c^{2m}\cos\varphi^{2m} + a^{2m}c^{2m}\sin\varphi^{2m}) - a^{2m}b^{2m}\cos\theta^{2m-1}\sin\theta], \tag{A14}$$

$$f_\varphi(\theta,\varphi) = 2m\sin\theta^{2m}[a^{2m}c^{2m}\sin\varphi^{2m-1}\cos\varphi - b^{2m}c^{2m}\cos\varphi^{2m-1}\sin\varphi], \tag{A15}$$

$$\begin{aligned} f_{\theta\theta}(\theta,\varphi) = {} & 2m\{[(2m-1)\sin\theta^{2m-2}\cos\theta^2 - \sin\theta^{2m}](b^{2m}c^{2m}\cos\varphi^{2m} + a^{2m}c^{2m}\sin\varphi^{2m}) \\ & + a^{2m}b^{2m}[(2m-1)\cos\theta^{2m-2}\sin\theta^2 - \cos\theta^{2m}]\}, \end{aligned} \tag{A16}$$

$$\begin{aligned} f_{\varphi\varphi}(\theta,\varphi) = {} & 2m\sin\theta^{2m}\{a^{2m}c^{2m}[(2m-1)\sin\varphi^{2m-2}\cos\varphi^2 - \sin\varphi^{2m}] \\ & + b^{2m}c^{2m}[(2m-1)\cos\varphi^{2m-2}\sin\varphi^2 - \cos\varphi^{2m}]\}, \end{aligned} \tag{A17}$$

$$f_{\theta\varphi}(\theta,\varphi) = 4m^2\sin\theta^{2m-1}\cos\theta[a^{2m}c^{2m}\sin\varphi^{2m-1}\cos\varphi - b^{2m}c^{2m}\cos\varphi^{2m-1}\sin\varphi]. \tag{A18}$$

[1] S. Torquato, *Random Heterogeneous Materials: Microstructure and Macroscopic Properties* (Springer, New York, 2002).

[2] A. Hunt, R. Ewing, and B. Ghanbarian, *Percolation Theory for Flow in Porous Media* (Springer, Heidelberg, 2014).

[3] D. S. McLachlan, T. B. Doyle, and G. Sauti, J. Magn. Magn. Mater. **458**, 365 (2018).

[4] G. T. Wang, C. Y. Wang, F. L. Zhang, and X. Z. Yu, Comput. Mater. Sci. **150**, 102 (2018).

[5] O. Gereben and L. Pusztai, Chem. Phys. **496**, 1 (2017).

[6] B. L. Xu, D. G. Shao, X. Z. Tan, X. Yang, W. Q. Gu, and H. X. Li, Agric. Water. Manage. **192**, 149 (2017).

[7] A. Chakhmane, H. Elidrissi, and A. Elkaaouachi, Mol. Cryst. Liq. Cryst. **627**, 92 (2016).

[8] D. P. Bentz, Cem. Concr. Compos. **31**, 285 (2009).

[9] Z. H. Ping, M. Zhong, Z. L. Long, X. J. Xu, G. K. Liao, and H. Chen, J. Non-Cryst. Solids. **488**, 14 (2018).

[10] A. G. Hunt and M. Sahimi, Rev. Geophys. **55**, 993 (2017).

[11] https://en.wikipedia.org/wiki/Percolation_threshold#Thresholds_for_3D_continuum_models.

[12] W. X. Xu, F. Wu, Y. Jiao, and M. Liu, Mater. Design **127**, 162 (2017).

[13] J. Q. Gan, A. B. Yu, and Z. Y. Zhou, Chem. Eng. Sci. **156**, 64 (2016).

[14] W. X. Xu, Z. Lv, and H. S. Chen, Phys. A (Amsterdam, Neth.) **392**, 416 (2013).

[15] W. X. Xu and H. S. Chen, Mater. Charact. **66**, 16 (2012).

[16] Z. G. Zhu and H. S. Chen, Powder Technol. **313**, 218 (2017).

[17] L. Liu, D. J. Shen, H. S. Chen, and W. X. Xu, Comput. Struct. **144**, 40 (2014).

[18] W. X. Xu and H. S. Chen, Modell. Simul. Mater. Sci. Eng. **20**, 075003 (2012).

[19] H. S. Chen, Z. G. Zhu, L. Liu, W. Sun, and C. W. Miao, Powder Technol. **289**, 1 (2016).

[20] Z. G. Zhu, J. L. Provis, and H. S. Chen, Powder Technol. **326**, 168 (2018).

[21] Z. G. Zhu, H. S. Chen, W. X. Xu, and L. Liu, Modell. Simul. Mater. Sci. Eng. **22**, 035008 (2014).
[22] D. J. Audus, A. M. Hassan, E. J. Garboczi, and J. F. Douglas, Soft Matter **11**, 3360 (2015).
[23] Y. Jiao, F. H. Stillinger, and S. Torquato, Phys. Rev. E **79**, 041309 (2009).
[24] J. M. Meijer, A. Pal, S. Ouhajji, H. N. W. Lekkerkerker, A. P. Philipse, and A. V. Petukhov, Nat. Commun. **8**, 14352 (2017).
[25] W. X. Xu, Z. M. Han, L. Tao, Q. H. Ding, and H. F. Ma, Powder Technol. **323**, 301 (2018).
[26] M. D. Rintoul and S. Torquato, J. Phys A: Math. Gen. **30**, L585 (1997).
[27] C. D. Lorenz and R. M. Ziff, J. Chem. Phys. **114**, 3659 (2001).
[28] A. M. Mascioli, C. J. Burke, M. Q. Giso, and T. J. Atherton, Soft Matter **13**, 7090 (2017).
[29] F. Azhari and N. Banthia, J. Mater. Sci. **50**, 5817 (2015).
[30] K. Meeks, M. L. Pantoya, M. Green, and J. Berg, Appl. Math. Modell. **46**, 116 (2017).
[31] E. J. Garboczi, K. A. Snyder, J. F. Douglas, and M. F. Thorpe, Phys. Rev. E **52**, 819 (1995).
[32] Y. B. Yi and A. M. Sastry, Proc. R. Soc. A **460**, 2353 (2004).
[33] E. Pervago, A. Mousatov, E. Kazatchenko, and M. Markov, Comput. Geosci. **116**, 53 (2018).
[34] C. Y. Zhang, X. L. Jian, and W. Lu, Soft Matter **11**, 1362 (2015).
[35] W. X. Xu, X. L. Su, and Y. Jiao, Phys. Rev. E **94**, 032122 (2016).
[36] S. Torquato and Y. Jiao, Phys. Rev. E **87**, 022111 (2013).
[37] B. Y. Ni, I. Elishakoff, C. Jiang, C. M. Fu, and X. Han, Appl. Math. Modell. **40**, 9427 (2016).
[38] S. W. Zhao, N. Zhang, X. W. Zhou, and L. Zhang, Powder Technol. **310**, 175 (2017).
[39] G. W. Delaney and P. W. Cleary, EPL **89**, 34002 (2010).
[40] W. X. Xu and H. S. Chen, Powder Technol. **221**, 296 (2012).
[41] Y. L. Wu, X. Z. An, and A. B. Yu, Powder Technol. **314**, 89 (2017).
[42] B. Zhao, X. Z. An, Y. Wang, Q. Qian, X. H. Yang, and X. D. Sun, Powder Technol. **317**, 171 (2017).
[43] W. X. Xu, H. S. Chen, and Z. Lv, Phys. A (Amsterdam, Neth.) **390**, 2452 (2011).
[44] J. J. Lin and H. S. Chen, Powder Technol. **335**, 388 (2018).
[45] X. S. Lin and T. T. Ng, Int. J. Numer. Anal. Meth. Geomech. **19**, 653 (1995).
[46] W. Zhou, Y. Huang, T. T. Ng, and G. Ma, Powder Technol. **327**, 152 (2018).
[47] P. W. Cleary, N. Stokes, and J. Hurley, in *Proceedings of 8th International Computational Techniques and Applications Conference (CTAC97)* (University of Adelaide, Adelaide, Australia, 1997), pp. 139–144.
[48] C. Wellmann, C. Lillie, and P. Wriggers, Eng. Comput. **25**, 432 (2008).
[49] S. W. Zhao and X. W. Zhou, Granular Matter **19**, 38 (2017).
[50] W. X. Xu, H. S. Chen, and Z. Lv, J. Wuhan Univ. Technol., Mater. Sci. Ed. **25**, 717 (2010).
[51] C. D. Lorenz and R. M. Ziff, J. Phys A: Math. Gen. **31**, 8147 (1998).
[52] M. E. J. Newman and R. M. Ziff, Phys. Rev. E **64**, 016706 (2001).
[53] J. F. Wang, Z. Z. Zhou, W. Zhang, T. M. Garoni, and Y. J. Deng, Phys. Rev. E **87**, 052107 (2013).
[54] H. Hu, H. W. J. Blöte, R. M. Ziff, and Y. J. Deng, Phys. Rev. E **90**, 042106 (2014).
[55] S. Torquato and Y. Jiao, J. Chem. Phys. **137**, 074106 (2012).
[56] I. Balberg, Phys. Rev. B **31**, 4053 (1985).